Journal of Mathematical Chemistry 15 (1994) 35–62

A left-right classification of topologically chiral knots

Chengzhi Liang and Kurt Mislow

Department of Chemistry, Princeton University, Princeton, NJ 08544, USA

Received 15 June 1993; revised 16 August 1993

A method for partitioning topologically chiral knots into mutually heterochiral classes has been developed, based on the principle that for such knots there exist no diagrams whose vertex-bicolored graphs are composed of equivalent black and white subgraphs. The method, which introduces the concept of *writhe profiles*, is successfully applied to alternating as well as non-alternating prime and composite knots, and works in cases where the Jones and Kauffman polynomials fail to recognize the knot's chirality. It is shown that writhe profiles are sensitive indicators of diagram similarity.

1. Introduction

The development of a well-founded scheme for partitioning topologically chiral knots into "right-handed" and "left-handed" classes has remained a challenging problem awaiting a satisfactory solution. The problem has been to discover a way of assigning any given knot to one of two homochiral, but mutually heterochiral, classes, so that any two knots in each class are "homochirally similar" [1,2], in the manner of "two equal and similar right hands" [1]. The homochirality concept [2] is strictly applicable because topologically chiral enantiomorphs cannot be interconverted by continuous deformation.

The challenge was faced for the first time in 1963, by Tauber [3]. Tauber's scheme was based on the conjecture, subsequently proven to be true [4,5], that the reduced diagrams of all topologically achiral (amphicheiral) alternating knots have an equal number of over- and undercrossings. If each of the crossing points in a knot K is assigned a characteristic ϵ with a value of $+1$, or -1, according to the convention in fig. 1, then the writhe $w(K)$ of such a knot, which is defined as the arithmetic sum $\Sigma\epsilon$, must always be zero. It follows immediately that if the writhe is not zero, then the alternating knot is topologically chiral. Furthermore, because over- and undercrossings are switched upon reflection in the plane of projection, it also follows that the writhe of a chiral knot and that of its enantiomorph are oppositely signed. Tauber used the convention in fig. 1 (though with the signs switched) to calculate $\Sigma\epsilon$ values for several topologically chiral and achiral knots, and proposed that the absolute configuration of a knot be designated R if $\Sigma\epsilon > 0$ and S if $\Sigma\epsilon < 0$, using the descriptors of the Cahn–Ingold–Prelog convention [6]. In support of his

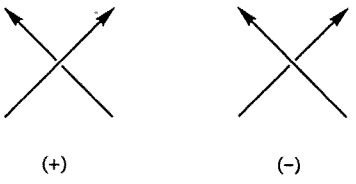

Fig. 1. Convention used to assign characteristics ($\epsilon = +1$ or -1) to crossings in knot diagrams.

proposal, Tauber pointed out that "For certain knots $\Sigma\epsilon = 0$. This is exactly as it should be, for precisely these knots are identical with their mirror images".

Tauber's scheme seems to have been generally accepted; for example, see [7]. In 1985, Walba [8] reported a convention for the specification of chirality in knots that was in all essential respects the same as Tauber's, except that $\epsilon = \delta$ or λ, instead of $+1$ and -1, and that the chirality descriptors were Δ and Λ, instead of R and S. "The number of δs and λs are then summed arithmetically. If there are the same number of δ and λ crossings, then the knot must be topologically achiral. If there are more λ crossings, the knot has configuration Λ. If there are more δ crossings, the knot is Δ."

There is, however, a fatal flaw in these schemes: *a writhe of zero is a necessary but not a sufficient condition for the amphicheirality of alternating knots.* As Flapan [5] has pointed out, the alternating composite knot $5_1\#5_2^*$, with $w(5_1) = -5$ and $w(5_2^*) = +5$, has writhe 0 even though it is topologically chiral. Actually, there are plenty of alternating *prime* knots with writhe 0 that are topologically chiral: the simplest of these is 8_4. Nineteen of the 32 10-crossing prime knots with writhe 0 are chiral, and 13 of these are alternating [9]. Two hundred sixty-two of the 320 12-crossing prime knots with writhe 0 are chiral, and 159 of these are alternating [10]. Furthermore, a writhe of zero may not even be a *necessary* condition for non-alternating amphicheiral knots: for example, the product knot $P_1\#P_2^*$ composed of a Perko pair with $w(P_1) = +10$ and $w(P_2^*) = -8$ (fig. 2) has writhe $+2$ even though it is topologically achiral. This knot can be isotoped to its mirror image, $P_1^*\#P_2$, with writhe -2, or to composite knots $P_1\#P_1^*$ and $P_2\#P_2^*$, both with writhe 0.

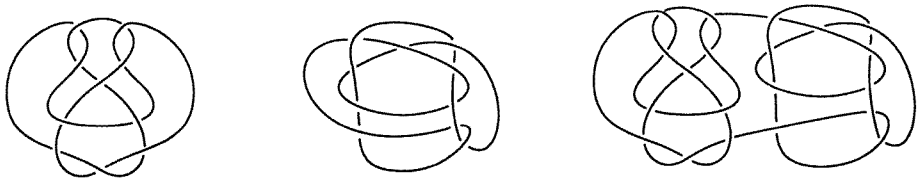

Fig. 2. Left and center: reduced diagrams of the "Perko pair", with writhes $+10$ (P_1, center) and $+8$ (P_2, left). P_1 and P_2 are isotopic (homeotopic) presentations of the same topologically chiral and non-alternating 10-crossing knot. Right: the composite amphicheiral knot $P_1\#P_2^*$ (P_2^* is obtained from P_2 by reflection in the plane of projection).

In the present paper we propose a scheme for partitioning topologically chiral knots into heterochiral classes that is applicable to alternating as well as to non-alternating prime and composite knots, *including those with writhe 0*.

2. A hierarchical order of writhes

A knot is amphicheiral if and only if the vertex-bicolored graph [11] of at least one of its reduced diagrams is composed of equivalent black and white subgraphs, inclusive of connectivities [12]; we refer to this as the *standard diagram*. Note that, according to this criterion, the diagrams of $P_1 \# P_1^*$ or $P_2 \# P_2^*$, but not of $P_1 \# P_2^*$ or $P_1^* \# P_2$, qualify as "standard". Fig. 3 illustrates this principle for a few selected prime knots. This equivalence is also expressed in the twofold antisymmetry of the corresponding adjacency matrix and in the condition that the derived polynomial satisfies $P(t) = P(t^{-1})$ [12].

In contrast, the corresponding subgraphs in topologically chiral knots are not equivalent even when the writhe of the knot is zero. That is, for any given black (white) vertex in the vertex-bicolored graph of such a knot, there exists no equiva-

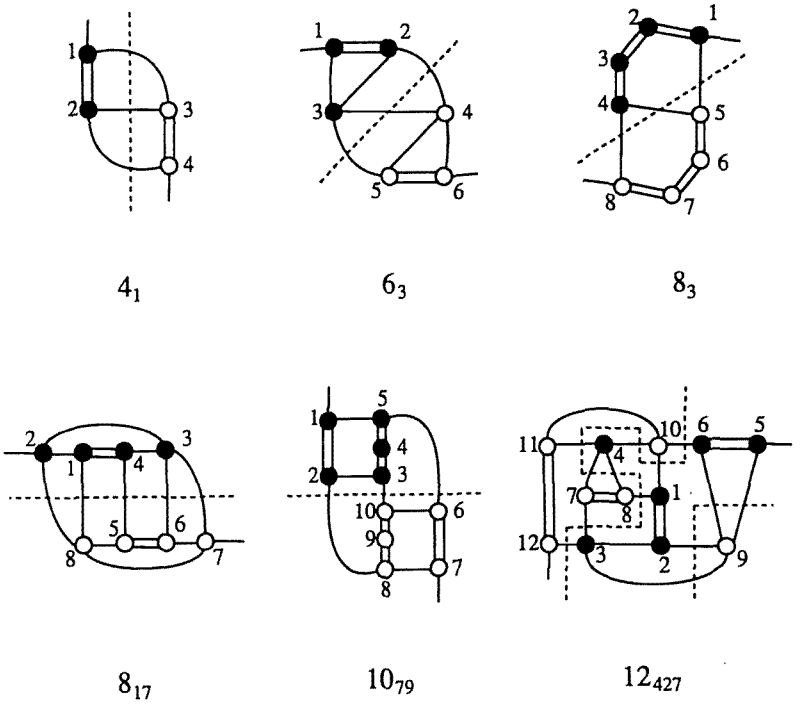

Fig. 3. A sampling of amphicheiral prime knots, with equivalent black and white subgraphs of the vertex-bicolored graphs separated by dashed lines. The filled (black) and open (white) circles represent the crossing point characteristics $\epsilon = +1$ and -1, respectively. The twofold antisymmetry of 12_{427} is "concealed" [12].

lent white (black) vertex. Accordingly, the *environment* of each black (white) vertex in such a graph has no counterpart among the white (black) vertices. This concept, which is at the heart of our scheme, is akin to the idea of atomic topicity introduced earlier in a chemical context [13]. In what follows, all references to crossing points and arcs of the knot apply with equal force to the vertices and edges of the corresponding knot graph.

2.1. TWO APPROACHES TO GAUGING CROSSING POINT OR VERTEX ENVIRONMENTS

Frank [14] has described two types of adjacency matrices for graphs: those whose elements a_{ij} give the number of edges that connect vertices i and j ("arc frequency matrix") and those whose elements are equal to 1 or 0 according to whether or not vertices i and j are connected by at least one edge ("arc indicator matrix"). For purposes of the present discussion we adopt Frank's terminology and refer to a given graph as a *frequency graph* if all multiple edges are included, and as an *indicator graph* if all multiple edges are replaced by single edges.

On the basis of this distinction, we have investigated two methods for gauging the environments of crossing points in reduced knot diagrams (or of vertices in the corresponding graphs). Both yield hierarchical ordering of writhes, but, as will be shown, in other respects the two methods give dramatically different results.

2.1.1. Frequency graphs

Conventional knot graphs, being regular of degree 4 [15], are frequency graphs. The following illustrates our method for a graph of this type. Consider a topologically chiral knot with a nonzero writhe, for example 7_6 (writhe -3), and its ith crossing point, for example the one that corresponds to vertex 1 in the knot graph (fig. 4). Let us imagine a set of concentric spherical shells $S_p, p = 0, 1, 2, \ldots$, with vertex 1 at the center ($p = 0$) and the three adjacent vertices, i.e. the nearest neighbors of vertex 1, placed on the nearest shell, S_1 (fig. 4) and connected to vertex 1 by single or double edges.

We define the pth-order characteristic $\epsilon_{i(p)}$ of the ith vertex as the sum of the zeroth-order characteristics of all the vertices j_p on S_p by eq. (1), where p is the length of the path from i to j_p and m is the number of double edges along that path.

$$\epsilon_{i(p)} = \sum_{j_p} 2^m \epsilon_{j_p(0)}, \quad p = 0, 1, 2, 3, \ldots . \tag{1}$$

According to eq. (1), $\epsilon_{1(0)} = -1$, i.e., the zeroth-order characteristic as conventionally defined. The characteristic of the first-order local environment of vertex 1 is given by $\epsilon_{1(1)} = \epsilon_{2(0)} + \epsilon_{6(0)} + 2\epsilon_{7(0)} = -2$; $\epsilon_{7(0)}$ is counted twice because there is one double edge joining vertices 1 and 7 ($m = 1$). In turn, the local environments of the three nearest neighbors are given by the characteristics of their adjacent vertices, which are placed on the next shell, S_2 (fig. 4); note that duplication of the

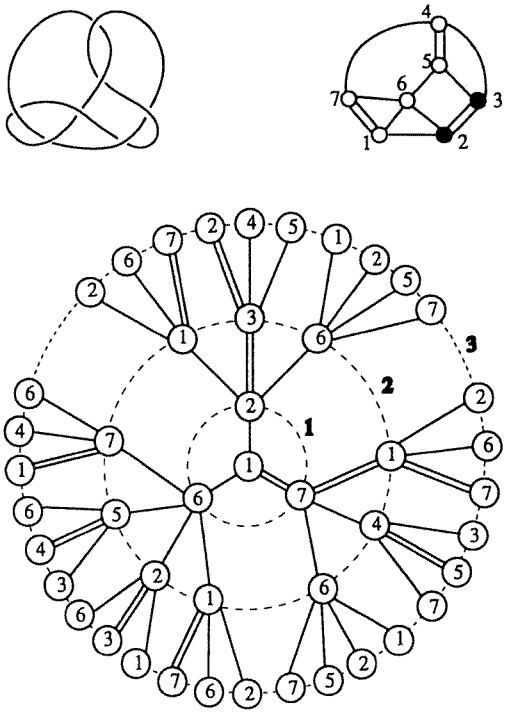

Fig. 4. Top left: reduced diagram of 7_6 [9]. Top right: the corresponding vertex-bicolored graph with numbered vertices. Bottom: a concentric-shell diagram showing three pth order environments (bold-faced numerals) of vertex 1 at the center ($p = 0$).

"inner" vertex 1 is necessary for a full accounting. The characteristic of the second-order local environment of vertex 1 is thus given by $\epsilon_{1(2)} = 6\epsilon_{1(0)} + \epsilon_{2(0)} + 2\epsilon_{3(0)} + 2\epsilon_{4(0)} + \epsilon_{5(0)} + 3\epsilon_{6(0)} + \epsilon_{7(0)} = -10$. Proceeding further (see fig. 4), the characteristic of the third-order local environment of vertex 1 is given by $\epsilon_{1(3)} = 6\epsilon_{1(0)} + 13\epsilon_{2(0)} + 5\epsilon_{3(0)} + 5\epsilon_{4(0)} + 9\epsilon_{5(0)} + 9\epsilon_{6(0)} + 17\epsilon_{7(0)} = -28$. The characteristics of the pth-order local environments of the other six vertices are similarly derived. In general,

$$\epsilon_{i(p)} = \sum_{k=1}^{N} r_{k,i(p)}\epsilon_{k(0)}, \quad p = 0, 1, 2, 3, \ldots , \tag{2}$$

where $r_{k,i(p)}$ is the contribution (or coefficient) of vertex k to $\epsilon_{i(p)}$.

We define the pth-order writhe w_p of a knot as the sum of the $\epsilon_{i(p)}$'s of all N crossing points in the knot:

$$w_p = \sum_{i=1}^{N} \epsilon_{i(p)}, \quad p = 0, 1, 2, 3, \ldots . \tag{3}$$

Table 1 lists the $\epsilon_{i(p)}$'s of all seven crossing points in knot 7_6, as well as the corre-

Table 1
pth-Order characteristics and writhes for knot 7_6 as determined by the frequency-graph method.

p	$\epsilon_{1(p)}$	$\epsilon_{2(p)}$	$\epsilon_{3(p)}$	$\epsilon_{4(p)}$	$\epsilon_{5(p)}$	$\epsilon_{6(p)}$	$\epsilon_{7(p)}$	w_p
0	−1	+1	+1	−1	−1	−1	−1	−3
1	−2	0	0	−2	−2	−2	−4	−12
2	−10	−4	−4	−8	−6	−8	−8	−48
3	−28	−26	−22	−24	−28	−28	−36	−192
4	−126	−100	−104	−114	−98	−118	−108	−768
5	−434	−452	−412	−408	−450	−432	−484	−3072

Table 2
pth-Order writhes of knots with $w_0 \neq 0$ as determined by the frequency-graph method.

w_0	w_1	w_2	w_3	w_4	w_5	Examples [a]
1	4	16	64	256	1024	$7_7, 9_8^*, 9_{42}$
2	8	32	128	512	2048	$6_1^*, 8_7, 10_{22}$
3	12	48	192	768	3072	$3_1^*, 7_6^*, 9_{14}$
4	16	64	256	1024	4048	$8_1^*, 10_{12}, 10_{130}^*$
5	20	80	320	1280	5120	$5_1^*, 5_2^*, 9_{11}$
6	24	96	384	1536	6144	$10_1^*, 10_{56}, 10_{150}$
		... ...				
N	4N	16N	64N	256N	1024N	

[a] Diagrams are taken from Rolfsen [9], with an asterisk denoting the enantiomorph of the drawing in [9]. For this set, all listed values are positive.

Table 3
pth-Order characteristics and writhes for knot 7_6 as determined by the indicator-graph method.

p	$\epsilon_{1(p)}$	$\epsilon_{2(p)}$	$\epsilon_{3(p)}$	$\epsilon_{4(p)}$	$\epsilon_{5(p)}$	$\epsilon_{6(p)}$	$\epsilon_{7(p)}$	w_p
0	−1	+1	+1	−1	−1	−1	−1	−3
1	−1	−1	−1	−1	−1	−2	−3	−10
2	−6	−4	−3	−5	−4	−6	−4	−32
3	−14	−15	−13	−11	−14	−18	−17	−102
4	−50	−45	−40	−44	−42	−60	−43	−324
5	−148	−150	−131	−125	−144	−180	−154	−1032

sponding w_p's up to w_5. The conventional (i.e. zeroth order) writhe (w_0) is -3, and as p increases so does the absolute magnitude of w_p, while the sign remains the same. Note that for $p \geqslant p_{\min} = 2$, all seven $\epsilon_{i(p)}$'s bear the same sign. In general, for every knot there exists a $p_{\min}$ such that all $\epsilon_{i(p)}$ components of w_p bear the same sign for $p \geqslant p_{min}$. Obviously, $p_{min} = 0$ if and only if all $\epsilon_{i(0)}$'s have the same sign (the trefoil knot is the simplest example).

The w_p's of 7_6 are shared by all knots with $w_0 = -3$. A different set of w_p's is shared by all knots with, say, $w_0 = 2$. In general, $w_p/w_0 = 4^p$ (table 2). This relation is a special case of the theorem in eq. (4).

THEOREM

If a graph is regular of degree q, then its pth-order writhe w_p satisfies

$$w_p = w_0 q^p, \quad p = 0, 1, 2, 3, \ldots . \tag{4}$$

Proof

Substituting $\epsilon_{i(p)}$ in eq. (3) by eq. (2), it is easy to see that

$$w_p = \sum_{k=1}^{N} g_{k(p)} \epsilon_{k(0)}, \quad p = 0, 1, 2, 3, \ldots , \tag{5}$$

where

$$g_{k(p)} = \sum_{i=1}^{N} r_{k,i(p)}, \quad p = 0, 1, 2, 3, \ldots ,$$

is equal to the number of paths of length p (or spanned p single edges) that are connected to vertex k.

Consider a regular graph of degree q. Any edge with multiplicity $h > 1$ can always be decomposed into h single edges so that every vertex in such a graph is the common terminal (or root) vertex of q q-regular trees [14]. At the pth stage (corresponding to S_p) of q q-regular trees with a common terminal vertex k, $g_{k(p)} = q^p$. Substitution of $g_{k(p)}$ in eq. (5) by q^p, in combination with eq. (3), yields eq. (4). □

2.1.2. Indicator graphs

Let us again apply the procedure described above for knot 7_6, but with one crucial difference: we now ignore the distinction between single and double edges. That is, the knot will be represented by an indicator rather than by a frequency graph. To borrow a concept from chemistry, we treat each vertex as a coordination center whose coordination number (δ) is given by the number of nearest "bonded" neighbors. In this view, six of the seven vertices in the knot graph of 7_6 have $\delta = 3$, and only vertex 6 has $\delta = 4$.

Eq. (1) is still valid, with the restriction that $m = 0$ throughout. That is, all double edges in the knot graph are, in effect, replaced by single edges. Accordingly,

$\epsilon_{1(0)} = -1$, $\epsilon_{1(1)} = \epsilon_{2(0)} + \epsilon_{6(0)} + \epsilon_{7(0)} = -1$, $\epsilon_{1(2)} = 3\epsilon_{1(0)} + \epsilon_{2(0)} + \epsilon_{3(0)} + \epsilon_{4(0)} + \epsilon_{5(0)} + 2\epsilon_{6(0)} + \epsilon_{7(0)} = -6$, and $\epsilon_{1(3)} = 4\epsilon_{1(0)} + 6\epsilon_{2(0)} + 3\epsilon_{3(0)} + 3\epsilon_{4(0)} + 4\epsilon_{5(0)} + 6\epsilon_{6(0)} + 6\epsilon_{7(0)} = -14$. The characteristics of the pth-order local environments of the other six vertices are similarly derived. Table 3 lists the $\epsilon_{i(p)}$'s of all seven crossing points in knot 7_6 as determined by this method, as well as the corresponding w_p's up to w_5. As was found in the frequency-graph approach (table 1), the absolute magnitude of w_p increases with an increase in p while the sign remains the same. The rates of increase, however, are very different, and now $p_{\min} = 1$.

That the two methods yield different results is to be expected, since identical results can be obtained only if the knot graph has no double edges. Of the 249 prime knots with up to 10 crossings depicted in [9] (the "classical" knots), only four have this property, and two of these (8_{18} and 10_{123}) are amphicheiral (fig. 5). The

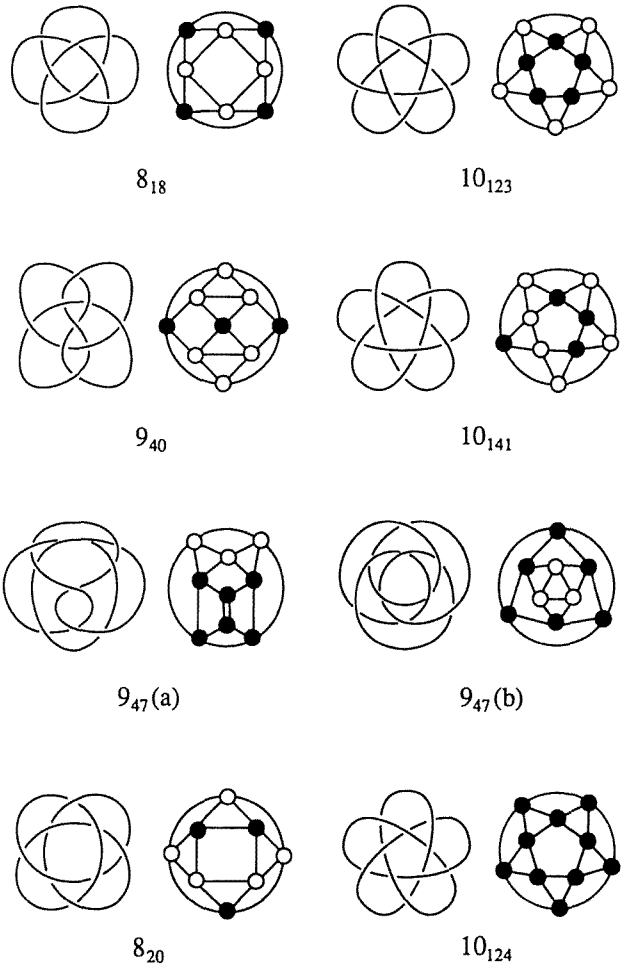

Fig. 5. Reduced diagrams and vertex-bicolored graphs of some classical prime knots with no double arcs. The top four diagrams are from [9] and the bottom two from [17]. Two diagrams are shown for 9_{47}: (a) with one double arc (from [9]) and (b) without double arcs (enantiomorph of [16]).

Table 4
pth-Order characteristics and writhes for knot 3_1 as determined by the indicator-graph method.

p	$\epsilon_{1(p)}$	$\epsilon_{2(p)}$	$\epsilon_{3(p)}$	w_p
0	−1	−1	−1	−3
1	−2	−2	−2	−6
2	−4	−4	−4	−12
3	−8	−8	−8	−24
4	−16	−16	−16	−48
5	−32	−32	−32	−96

two topologically chiral knots in [9] with no double arcs are 9_{40} and 10_{141} (fig. 5), and the two methods give the same set of pth-order writhes for each knot (table 2: $w_0 = 3$ for 9^*_{40} and $w_0 = 2$ for 10^*_{141}). Diagrams with this property are, however, by no means restricted to the four listed above, as exemplified by 9_{47} (fig. 5(b) [16]). Additional examples are found in the work of Tait [17] (fig. 5: 8_{20} (whose enantiomorph is known as the "bowline knot" [18]) and 10_{124}).

There are two decisive reasons why the indicator-graph approach is the only

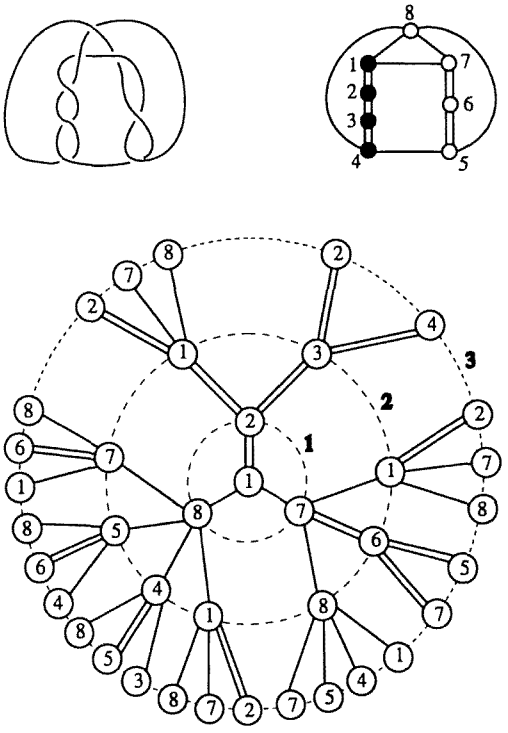

Fig. 6. Top left: reduced diagram of 8_4 [9]. Top right: the corresponding vertex-bicolored graph with numbered vertices. Bottom: a concentric-shell diagram showing three pth order environments (bold-faced numerals) of vertex 1 at the center ($p = 0$).

Table 5
pth-Order characteristics and writhes for knot 8_4 as determined by the indicator-graph method.

p	$\epsilon_{1(p)}$	$\epsilon_{2(p)}$	$\epsilon_{3(p)}$	$\epsilon_{4(p)}$	$\epsilon_{5(p)}$	$\epsilon_{6(p)}$	$\epsilon_{7(p)}$	$\epsilon_{8(p)}$	w_p
0	+1	+1	+1	+1	−1	−1	−1	−1	0
1	−1	+2	+2	−1	−1	−2	−1	0	−2
2	+1	+1	+1	+1	−3	−2	−3	−4	−8
3	−6	+2	+2	−6	−5	−6	−5	−4	−28
4	−7	−4	−4	−7	−16	−10	−16	−22	−86
5	−42	−11	−11	−42	−39	−32	−39	−46	−262

one that suits our purposes. First, this method allows differentiation among knots with the same w_0, as shown, for example, by a comparison of the results for 7_6 (table 3) and for the trefoil knot (table 4). This information is lost in the frequency-graph approach, which yields the same result for all knots with the same w_0 (table 2), even though it could hardly be argued that the combined local environments of knots such as 7_6 and 3_1 are the same.

The second reason is that the frequency-graph approach allows a hierarchical ordering of writhes only if $w_0 \neq 0$ because, according to eq. (4), $w_p = 0$ for *all* p's if $w_0 = 0$. This crippling limitation can be circumvented by resorting to indicator graphs. For example, if we apply the procedure described for 7_6 in this section to the topologically chiral knot 8_4 with $w_0 = 0$ (see fig. 6), we find that $\epsilon_{1(0)} = +1$, $\epsilon_{1(1)} = \epsilon_{2(0)} + \epsilon_{7(0)} + \epsilon_{8(0)} = -1$, $\epsilon_{1(2)} = 3\epsilon_{1(0)} + \epsilon_{3(0)} + \epsilon_{4(0)} + \epsilon_{5(0)} + \epsilon_{6(0)} + \epsilon_{7(0)} + \epsilon_{8(0)} = +1$, and $\epsilon_{1(3)} = 2\epsilon_{1(0)} + 4\epsilon_{2(0)} + \epsilon_{3(0)} + 3\epsilon_{4(0)} + 3\epsilon_{5(0)} + 2\epsilon_{6(0)} + 5\epsilon_{7(0)} + 6\epsilon_{8(0)} = -6$. Table 5 lists all the $\epsilon_{i(p)}$'s, as well as the corresponding w_p's up to w_5; $p_{\min} = 4$. The equivalences $\epsilon_{1(p)} = \epsilon_{4(p)}$, $\epsilon_{2(p)} = \epsilon_{3(p)}$, and $\epsilon_{5(p)} = \epsilon_{7(p)}$ arise from the fact that 8_4 can be projected as a diagram with C_2 symmetry in which crossing points 6 and 8 lie on the C_2 axis.

Thus, by use of this method, the nonequivalence of the black and white sub-

Table 6
Writhe profiles for representative knots with w_0's ranging from 0 to 10.

w_0	w_1	w_2	w_3	w_4	w_5	Example [9]
0	+2	+10	+40	+144	+498	10_{19}
+1	+4	+10	+32	+98	+316	9_{22}
+2	+4	+8	+18	+48	+140	8_7
+3	+4	+8	+18	+50	+150	9_{14}
+4	+10	+26	+74	+206	+582	8_5
+5	+14	+40	+118	+354	+1072	9_{11}
+6	+16	+44	+126	+356	+1020	10_{50}
+7	+20	+60	+180	+540	+1620	7_4
+8	+28	+100	+358	+1284	+4606	8_{19}
+9	+24	+68	+196	+570	+1664	9_5
+10	+34	+118	+410	+1428	+4972	10_{101}

graphs of a topologically chiral knot's vertex-bicolored graph is revealed even if the knot's writhe is zero. In what follows, all $\epsilon_{i(p)}$'s and w_p's are derived by this method.

For every knot, the indicator-graph method yields a series of ordered writhes, $w_0, w_1, \ldots, w_p$, which we call the *writhe profile* of the knot. If and only if the knot is amphicheiral, all w_p's are zero and the profile is a flat line. With the single exception of knot 7_7, which will be discussed below, the w_p's of all 229 non-amphicheiral classical prime knots increase monotonically in absolute value but without a change in sign, beginning with the smallest nonzero writhe, w_s, for all values of $p \geqslant s$. A representative sample is displayed in table 6. Thus the writhe profile of such a knot is a signed quantity. Obviously, $s = 0$ if and only if $w_0 \neq 0$; if $w_0 = 0$, then $s > 0$, as in the example of 8_4 ($s = 1$). Nor is the approach restricted to prime knots; for example, the composite knot $5_1 \# 5_2^*$ mentioned in the Introduction has $w_p = 0$, 2, 10, 36, 116, 352 for $p = 0$ through 5, with $s = 1$ and $p_{\min} = 7$, and the granny knot $3_1 \# 3_1$ has $w_p = -6, -16, -44, -120, -328$, and -896 for $p = 0$ through 5, with $s = 0$ and $p_{\min} = 0$.

2.1.3. The 7_7 syndrome

The monotonic increase in w_p's described above was observed in all cases but that of knot 7_7. From the reduced diagram in fig. 7(a), $w_p = 1, 0, 0, -2, -6, -24$, and -80 for $p = 0$ through 6 ($p_{\min} = 6$), while for the diagram in fig. 7(b), $w_p = 1, 0$, 4, 8, 38, 112, 436, 1408, and 5180 for $p = 0$ through 8 ($p_{\min} = 8$). The root cause of this aberrant behavior is evidently related to the fact that of all the 209 classical prime knots with nonzero writhe ($w_0 \neq 0$), 7_7 is unique in having $\Sigma\delta = 0$, where δ is now the *signed* coordination number. That is, with reference to fig. 7, $\delta_+ = 3$ and $\delta_- = -4$, hence $4\delta_+ + 3\delta_- = 0$.

If the purpose is to assign a knot's configuration (section 3), it is vital to avoid this condition, provided that there is a choice among diagrams from which to derive a writhe profile. An instructive example is provided by knot 9_{42} (fig. 8). The three diagrams (a)–(c), constructed from tangles in [19], give different results for the respective w_p's (table 7), but what is notable is that only (c) exhibits the 7_7 syn-

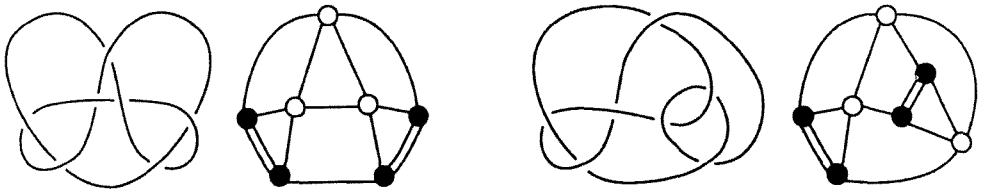

(a) (b)

Fig. 7. (a) Reduced diagram of 7_7 [9] and the corresponding vertex-bicolored graph. (b) An isotopic diagram of 7_7 and the corresponding graph.

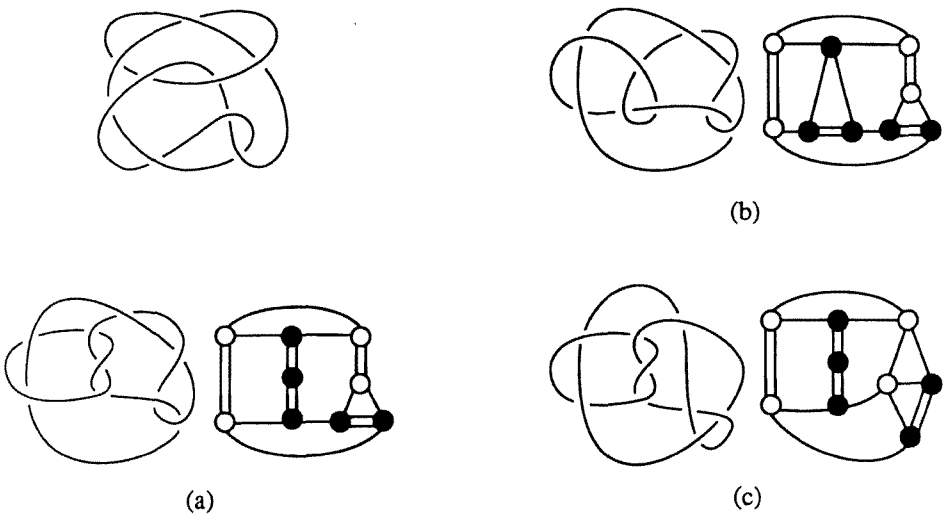

Fig. 8. Top left: reduced diagram of 9_{42} [9]. (a)–(c) Three isotopic diagrams of 9_{42} and the corresponding vertex-bicolored graphs. Graph (a) also represents the diagram at the top left.

drome. The signed $\Sigma\delta$'s are consistent with this behavior: $\Sigma\delta = +2, +4$, and 0 for (a), (b) and (c), respectively. The choice of diagrams suitable for a left-right classification is therefore limited to (a) or to (b).

2.2. SYMMETRIC AND ANTISYMMETRIC CROSSING POINT ENVIRONMENTS

Given the standard diagram of an amphicheiral knot, the black and white vertices of the corresponding vertex-bicolored graph are either pairwise symmetric, that is, related by twofold rotation, or pairwise antisymmetric, that is, related by twofold antirotation (i.e. twofold rotation combined with a transposition of colors [12]). The positive and negative component $\epsilon_{i(p)}$'s of all w_p's in the knot's standard diagram cancel exactly, so the w_p's are zero for all values of p.

In this section we show that symmetry and antisymmetry are revealed by an analysis of the characteristics of the local environments. Tables 8–13 list some pth-order characteristics for the six knots in fig. 3 (the numbers attached to the vertices in that figure correspond to the i's of the $\epsilon_{i(p)}$ values listed in the tables). We begin by examining table 13 (knot 12_{427}). Although the matched pairs cannot all be iden-

Table 7
Writhe profiles for knot 9_{42}.

graph [a]	w_0	w_1	w_2	w_3	w_4	w_5	w_6	w_7	$p_{\min}$
a	+1	+2	+4	+12	+32	+98	+278	+838	7
b	+1	+4	+12	+38	+120	+374	+1184	+3702	3
c	+1	0	0	−2	−6	−24	−72	−250	13

[a] See fig. 8.

Table 8
pth-Order characteristics for knot 4_1.

p	$\epsilon_{1(p)}$	$\epsilon_{2(p)}$	$\epsilon_{3(p)}$	$\epsilon_{4(p)}$
0	+1	+1	−1	−1
1	−1	−1	+1	+1
2	+1	+1	−1	−1
3	−1	−1	+1	+1

Table 9
pth-Order characteristics for knot 6_3.

p	$\epsilon_{1(p)}$	$\epsilon_{2(p)}$	$\epsilon_{3(p)}$	$\epsilon_{4(p)}$	$\epsilon_{5(p)}$	$\epsilon_{6(p)}$
0	+1	+1	+1	−1	−1	−1
1	+1	+1	0	0	−1	−1
2	0	+1	+1	−1	−1	0
3	+2	0	−1	+1	0	−2
4	−3	+2	+3	−3	−2	+3
5	+8	−3	−6	+6	+3	−8

Table 10
pth-Order characteristics for knot 8_3.

p	$\epsilon_{1(p)}$	$\epsilon_{2(p)}$	$\epsilon_{3(p)}$	$\epsilon_{4(p)}$	$\epsilon_{5(p)}$	$\epsilon_{6(p)}$	$\epsilon_{7(p)}$	$\epsilon_{8(p)}$
0	+1	+1	+1	+1	−1	−1	−1	−1
1	−1	+2	+2	−1	+1	−2	−2	+1
2	+4	+1	+1	+4	−4	−1	−1	−4
3	−7	+5	+5	−7	+7	−5	−5	+7

Table 11
pth-Order characteristics for knot 8_{17}.

p	$\epsilon_{1(p)}$	$\epsilon_{2(p)}$	$\epsilon_{3(p)}$	$\epsilon_{4(p)}$	$\epsilon_{5(p)}$	$\epsilon_{6(p)}$	$\epsilon_{7(p)}$	$\epsilon_{8(p)}$
0	+1	+1	+1	+1	−1	−1	−1	−1
1	+1	0	0	+1	−1	−1	0	0
2	+1	+1	0	0	0	−1	−1	0
3	+1	0	−1	+1	−1	−1	0	+1
4	+2	+1	0	−1	+1	−2	−1	0
5	0	+1	−3	+3	−3	0	−1	+3
6	+7	−1	+3	−6	+6	−7	+1	−3

Table 12
pth-Order characteristics for knot 10_{79}.

p	$\epsilon_{1(p)}$	$\epsilon_{2(p)}$	$\epsilon_{3(p)}$	$\epsilon_{4(p)}$	$\epsilon_{5(p)}$	$\epsilon_{6(p)}$	$\epsilon_{7(p)}$	$\epsilon_{8(p)}$	$\epsilon_{9(p)}$	$\epsilon_{10(p)}$
0	+1	+1	+1	+1	+1	−1	−1	−1	−1	−1
1	+1	+1	+1	+2	+1	−1	−1	−1	−2	−1
2	+1	+1	+2	+2	+2	−1	−1	−2	−2	−2
3	+2	+1	+1	+4	+2	−1	−2	−2	−4	−1
4	+1	+1	+4	+3	+5	−1	−1	−5	−3	−4
5	+5	0	0	+9	+3	0	−5	−3	−9	0
6	−2	+2	+9	+3	+14	−2	+2	−14	−3	−9
7	+18	−7	−4	+23	−1	+7	−18	+1	−23	+4

Table 13
pth-Order characteristics for knot 12_{427}.

p	$\epsilon_{1(p)}$	$\epsilon_{2(p)}$	$\epsilon_{3(p)}$	$\epsilon_{4(p)}$	$\epsilon_{5(p)}$	$\epsilon_{6(p)}$	$\epsilon_{7(p)}$	$\epsilon_{8(p)}$	$\epsilon_{9(p)}$	$\epsilon_{10(p)}$	$\epsilon_{11(p)}$	$\epsilon_{12(p)}$
0	+1	+1	+1	+1	+1	+1	−1	−1	−1	−1	−1	−1
1	−1	+1	−2	−4	−1	−1	+1	+1	+4	+2	−1	+1
2	+4	+1	+7	+3	+4	+5	−5	−4	−3	−7	−1	−4
3	−10	+8	−11	−17	−2	−6	+6	+2	+17	+11	−8	+10

tified from the $\epsilon_{i(p)}$'s given for $p = 0$, 1, or 2 in the table, the $\epsilon_{i(p)}$'s for $p = 3$ clearly display the antisymmetry ($\sim$) of all 6 pairs: $1 \sim 12$; $2 \sim 11$; $3 \sim 10$; $4 \sim 9$; $5 \sim 8$; $6 \sim 7$. A different situation is encountered in tables 9, 11, and 12: here, all antisymmetric pairs can be unambiguously identified before all the differences among them become explicit. Consider table 9 (knot 6_3). The antisymmetry of all 3 pairs ($1 \sim 6; 2 \sim 5; 3 \sim 4$) becomes evident only at $p = 3$ but can be unambiguously derived from the values in the first 3 rows ($p = 0, 1, 2$). In table 11 (knot 8_{17}), the antisymmetry of all 4 pairs ($1 \sim 6; 2 \sim 7; 3 \sim 8; 4 \sim 5$) is evident only at $p = 6$ but can also be derived from the first 3 rows. And in table 12 (knot 10_{79}), the antisymmetry of all 5 pairs ($1 \sim 7; 2 \sim 6; 3 \sim 10; 4 \sim 9; 5 \sim 8$) is evident only at $p = 7$ but can be derived from the first 4 rows.

Tables 8 and 10 present yet another set of relationships: now symmetrically paired vertices are antisymmetric relative to other such pairs. In table 8 (knot 4_1) this is already obvious at $p = 0$, which shows that vertices 1 and 2 are symmetric (,), as are vertices 3 and 4, so that $1, 2 \sim 3, 4$. Similarly, in table 10 (knot 8_3) it is clear at $p = 1$ that $1, 4 \sim 5, 8$ and $2, 3 \sim 6, 7$.

Finally, we note that this type of analysis fails if each vertex in the vertex-bicolored graph is surrounded by an equal number of white and black vertices, as is the case for knots 8_{18} and 10_{123} (fig. 5). In such a case, not only are all the w_p's zero, in common with all other amphicheiral knots, but so are all the $\epsilon_{i(p)}$'s. Accordingly, no information can be extracted concerning symmetric or antisymmetric relationships.

3. Classes of homochiral knots

The procedure to determine the desired classification consist of two steps. First the vertex-bicolored graph of the knot's reduced diagram is obtained (standard graphs for amphicheiral knots). Second, the knot's writhe profile is determined by use of the indicator-graph method. If all w_p's are zero, the knot is amphicheiral. Otherwise, the sign of the smallest nonzero writhe, w_s, suffices for the assignment of the knot to the appropriate class, according to the following definition:

DEFINITION

A knot is right-handed (denoted D) if $w_s > 0$, i.e. if the writhe profile is positive, and left-handed (denoted by L) if $w_s < 0$, i.e. if the writhe profile is negative.

For the great majority of topologically chiral knots, $w_s = w_0$. In such cases our scheme matches the schemes discussed in the Introduction, with D/L replacing R/S [3] and Δ/Λ [8]. Our definition also accords with the usual (if arbitrary) sign convention (fig. 1) that results, for example, in the common attribution of "right-handedness" and "left-handedness" to trefoil knots with $w_0 = +3$ and -3, respectively. For topologically chiral knots with $w_0 = 0$ (i.e. with $s > 0$), where previous schemes have failed our scheme now provides a ready answer: for such knots, the sense of chirality, hidden in the zeroth-order writhe, is revealed in the high-order writhes. This is illustrated in table 14 for all 20 classical chiral prime knots with writhe 0, and in table 15 for 32 of the 262 12-crossing chiral prime knots with writhe 0. The knots in table 15 were selected in order to demonstrate the applicability of our classification scheme even in cases where the Jones and Kauffman polynomials [20] fail to recognize the chirality of the knot. The diagrams of the 12-crossing knots in fig. 9 were developed from notation provided by Thistlethwaite [10,21].

Diagram polymorphism presents no problem: although writhe profiles are diagram-dependent, their signs are invariant for a given enantiomorph and are therefore suitable for the assignment of knots to their proper homochirality classes. For example, diagrams (a) and (b) for knot 9_{42} are different (fig. 8) and so are the

Table 14
Left-right classification of the 8- and 10-crossing chiral prime knots with $w_0 = 0$.

Knot [a]	w_0	w_1	w_2	w_3	w_4	w_5	p_{min}	D/L	Polynomial [b]
8_4	0	−2	−8	−28	−86	−262	4	L	
10_{15}	0	0	−2	−8	−30	−96	8	L	
10_{19}	0	+2	+10	+40	+144	+498	5	D	
10_{31}	0	+2	+8	+32	+110	+376	6	D	
10_{42}	0	+2	+6	+18	+56	+182	6	D	
10_{48}	0	0	+2	+10	+36	+118	7	D	V
10_{52}	0	−2	−8	−28	−92	−296	5	L	
10_{54}	0	0	0	0	−2	−8	15	L	
10_{71}	0	0	0	0	+2	+4	14	D	V, K
10_{91}	0	0	+2	+10	+36	+126	6	D	V
10_{93}	0	0	−2	−8	−28	−96	6	L	
10_{104}	0	0	+2	+10	+38	+138	5	D	V
10_{107}	0	+2	+10	+40	+150	+542	4	D	
10_{108}	0	0	+2	+6	+16	+42	10	D	
10_{125}	0	−2	−10	−34	−104	−302	5	L	V
10_{129}	0	−4	−18	−66	−232	−792	4	L	
10_{135}	0	0	−2	−10	−42	−158	8	L	
10_{146}	0	−2	−6	−20	−60	−184	6	L	
10_{153}	0	+2	+10	+36	+122	+388	4	D	
10_{165}	0	−2	−10	−42	−166	−646	6	L	

[a] All knot diagrams are from [9].

[b] "V" or "V, K" means that the Jones polynomial V or that both the Jones and the Kauffman polynomials K fail to detect the chirality of the corresponding knot. V and K polynomials were provided by Thistlethwaite [10].

Table 15
Left-right classification of selected 12-crossing chiral prime knots with $w_0 = 0$.

Knot [a]	w_0	w_1	w_2	w_3	w_4	w_5	p_{min}	D/L	Polynomial [b]
12_{2}	0	+2	+4	+16	+46	+154	6	D	
12_{99}	0	+2	+10	+40	+148	+540	6	D	
12_{126}	0	+2	+2	+22	+60	+292	9	D	V, K
12_{132}	0	+2	+4	+24	+74	+308	7	D	V, K
12_{214}	0	+4	+16	+60	+228	+846	4	D	V, K
12_{222}	0	0	+2	8	+36	+132	8	D	V, K
12_{453}	0	+2	+4	+20	+54	+210	12	D	V
12_{674}	0	+2	+4	+20	+58	+240	11	D	V
12_{697}	0	+4	+18	+74	+294	+1124	5	D	V, K
12_{778}	0	+2	+10	+42	+160	+592	5	D	
12_{943}	0	−4	−18	−74	−274	−994	5	L	V
12_{1007}	0	+2	+10	+38	+138	+484	6	D	
12_{1011}	0	0	+2	+12	+46	+162	7	D	V
12_{1081}	0	0	+2	+8	+30	+100	9	D	V
12_{1088}	0	0	0	+2	+8	+36	9	D	V
12_{1199}	0	0	−2	−10	−38	−136	7	L	V
12_{1222}	0	0	+2	+10	+40	+152	5	D	V
12_{1231}	0	0	+2	+10	+38	+136	7	D	V
12_{1235}	0	0	−2	−12	−48	−176	7	L	V
12_{1245}	0	+2	+8	+28	+96	+320	6	D	
12_{1250}	0	0	0	−2	−10	−48	10	L	V
12_{1258}	0	0	0	0	0	−2	16	L	V
12_{1283}	0	0	+2	+12	+46	+154	8	D	V
12_{1313}	0	0	−6	−22	−86	−278	6	L	
12_{1553}	0	+4	+16	+64	+224	+796	4	D	
12_{1746}	0	0	0	0	−8	−42	11	L	
12_{1794}	0	+2	+6	+20	+68	+236	6	D	V
12_{1848}	0	+2	+10	+40	+154	+572	6	D	
12_{1850}	0	+2	+12	+46	+186	+672	7	D	V
12_{1859}	0	+4	+22	+86	+314	+1074	6	D	V
12_{2109}	0	+4	+16	+58	+188	+610	4	D	V
12_{2173}	0	+2	+8	+30	+110	+400	7	D	

[a] Reduced diagrams of the knots are depicted in fig. 9.
[b] See table 14, footnote (b).

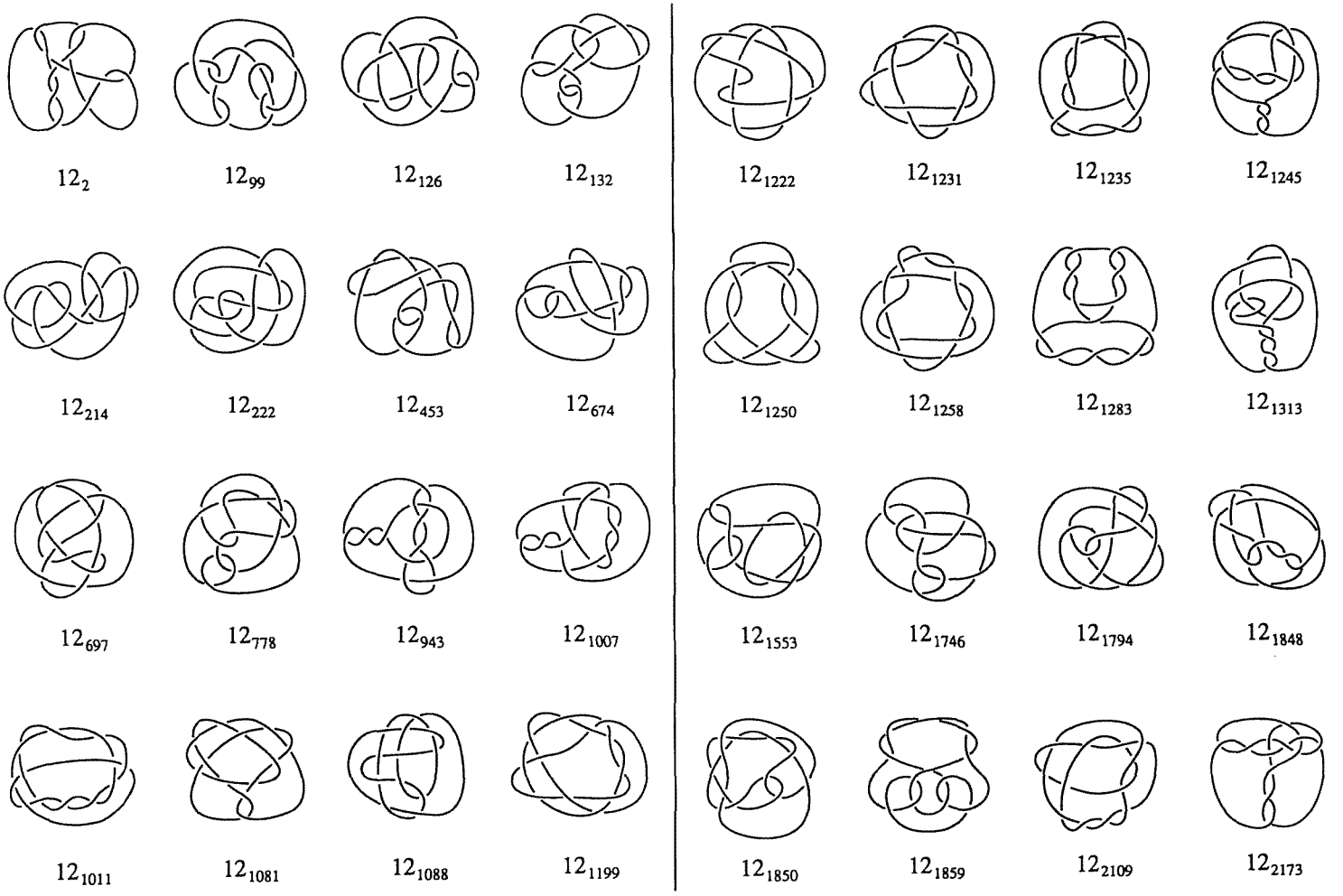

Fig. 9. Reduced diagrams of the 12-crossing knots in table 15.

Table 16
Parameters of linear plots for 13 sets of similar diagrams [a]

Knot [b]	w_0 [c]	w_s' [d]	$w_{19} \times 10^{-10}$ [e]	κ [f]	$\log f$ [g]
8_5 [h]	4	3.46	0.11	0.448	0.439
8_{19} [h]	8	7.85	0.27	0.449	0.439
8_{20}^* [i]	2	2.19	0.08	0.450	0.439
8_{19}	8	7.81	26.99	0.555	0.544
8_{20}^*	2	2.16	7.67	0.555	0.544
8_{21}^*	4	3.47	11.65	0.554	0.544
9_{22} [j]	1	0.86	0.38	0.505	0.493
9_{45}^*	5	3.71	1.74	0.508	0.493
9_{25}^*	5	5.23	1.56	0.499	0.493
9_{44}^* [j]	1	1.34	0.45	0.503	0.493
9_{45}^* [j]	5	5.06	1.46	0.498	0.493
9_{33}^* [j]	1	1.21	6.40	0.565	0.551
9_{44}^*	1	1.16	6.19	0.565	0.551
9_{36}	5	4.71	0.34	0.466	0.461
9_{43} [j]	5	4.70	0.33	0.465	0.461
9_{39}	5	5.23	7.48	0.535	0.523
9_{48}	5	4.07	5.34	0.532	0.523
9_{49}	9	8.76	12.27	0.534	0.523
10_{46}	6	4.68	0.09	0.435	0.415
10_{124} [k]	10	9.31	0.21	0.439	0.415
10_{126}^*	4	3.37	0.07	0.435	0.415
10_{52}^*	0 [l]	2.65	0.29	0.504	0.477
10_{130}^*	4	4.35	1.36	0.500	0.477
10_{131}^*	6	5.86	1.82	0.500	0.477
10_{113}	4	3.39	42.98	0.583	0.580
10_{132}^*	4	3.56	47.95	0.585	0.580
10_{133}^*	6	5.67	78.66	0.586	0.580
10_{134}	10	9.81	138.14	0.587	0.580
10_{136}	2	1.56	20.27	0.584	0.580
10_{147}	2	1.48	17.58	0.581	0.580
10_{150}	6	5.78	81.53	0.587	0.580
10_{120}^*	10	9.84	52.30	0.565	0.556
10_{166}	6	6.44	35.02	0.565	0.556
10_{137}^*	2	1.70	3.11	0.540	0.532
10_{138}	2	2.64	5.41	0.543	0.532

Table continued on next page

Table 16 (continued)

Knot [b]	w_0 [c]	w_s' [d]	$w_{19} \times 10^{-10}$ [e]	κ [f]	$\log f$ [g]
12^*_{29}	4	3.66	4.55	0.531	0.523
12_{1343}	4	4.56	5.99	0.533	0.523
12^*_{1345}	2	1.45	1.91	0.533	0.523
12^*_{1346}	8	7.15	8.76	0.531	0.523
12_{1347}	8	8.07	10.21	0.532	0.523
12_{1348}	2	2.38	3.35	0.535	0.523
12_{1349}	2	2.02	2.31	0.528	0.523

[a] Similar diagrams are defined as sharing the same knot graph. Diagrams of knots and their vertex-bicolored graphs are depicted in the D-configuration in figs. 10–15. The parameters listed in this table all correspond to linear plots with $R^2 = 1.000$.

[b] Notation for 12-crossing knots was supplied by Thistlethwaite [10]; all other knots were taken from Rolfsen [9] unless otherwise noted. An asterisk denotes the enantiomorph of the corresponding diagrams in [9,10].

[c] Zeroth-order (conventional) writhe.

[d] Antilog of the intercept on the $\log w_p$ axis (eq. (6)). While w_s must be an integer, w_s' is the smallest writhe that is compatible with a linear plot.

[e] Largest computed w_p value.

[f] Eq. (6).

[g] Eq. (7).

[h] Diagram from [18].

[i] Diagram from [17].

[j] Diagram isotopic to the one depicted in [9].

[k] The diagram has 7 double edges (fig. 15). Another diagram of the same knot, with no double edges (fig. 5), has a very different writhe profile (see table 2).

[l] $w_s = +2, s = 1$.

corresponding writhe profiles (table 7), but both profiles are positive and the knot is therefore assigned the D configuration. Another example is provided by knot 9_{47}; the writhe profiles for the diagrams in fig. 5(a) ($w_p = +3, +10, +34, +126, +474, +1808$ for $p = 0$ through 5) and fig. 5(b) (table 2: $w_0 = 3$) obviously differ, but both are positive and the knot therefore belongs to the D class. The same is true of the Perko pair in fig. 2: for $P_1, w_p = +10, +34, +118, +410, +1430, \ldots$, and for $P_2, w_p = +8, +24, +78, +254, +850, \ldots$. We have so far been unable to discover any ambiguities or contradictions, but, given the empirical nature of our investigation, further work may be required to test the limits of usefulness of the method.

4. Writhe profiles as indicators of diagram similarity

By eliminating all zero-valued w_p's from the writhe profiles of non-amphicheiral knots, eq. (4) may be restated, in modified form, as

$$\log w_p \approx \kappa(p - s) + \log w_s' . \tag{6}$$

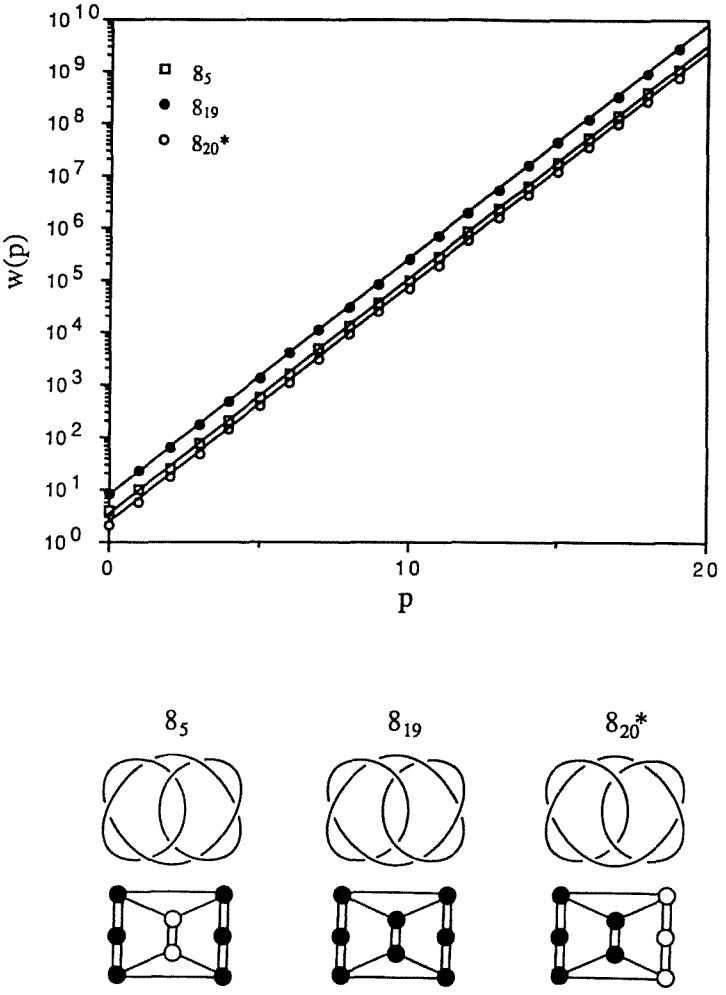

Fig. 10. Linear plot of eq. (6) ($s = 0$) for the illustrated set of similar knot diagrams and their vertex-bicolored graphs. Provenance of diagrams and parameters of plots are listed in table 16. Knot 8_5^* and the version of 8_{19}^* shown here are known as the "false lover's knot" and the "true lover's knot", respectively [18].

Eq. (6), which corresponds to a straight line with slope κ and intercept $\log w_s'$, is exact for regular graphs of degree q, with $w_s' = w_s = w_0$ and $\kappa = \log q$. Thus, knot graphs with no single edges (e.g. $3_1, 5_1, 7_1, 9_1$ [9]), those with two single edges and one double edge incident on each vertex (e.g. 10_{58} [9]), and those with no double edges (e.g. some graphs in fig. 5), yield linear plots of $\log w_p$ vs. p with slopes $\kappa = \log 2, \log 3$, and $\log 4$, respectively. In all other cases a linear relationship is closely approximated ($R^2 \geqslant 0.997$) with w_p's ranging over ca. 10 orders of magnitude

for all plots examined so far, and with $w_s' \approx w_s$. Parameters of 42 plots with $R^2 = 1.000$ are listed in table 16, and the corresponding knot diagrams and vertex-bicolored graphs are depicted in figs. 10–15.

Diagrams that are similar, in the sense that they share the same knot graph, yield linear plots with slopes that are the same to within ca. 1% or less (table 16, figs. 10–15). Figs. 10–14 display some of the plots and also illustrate the role played by

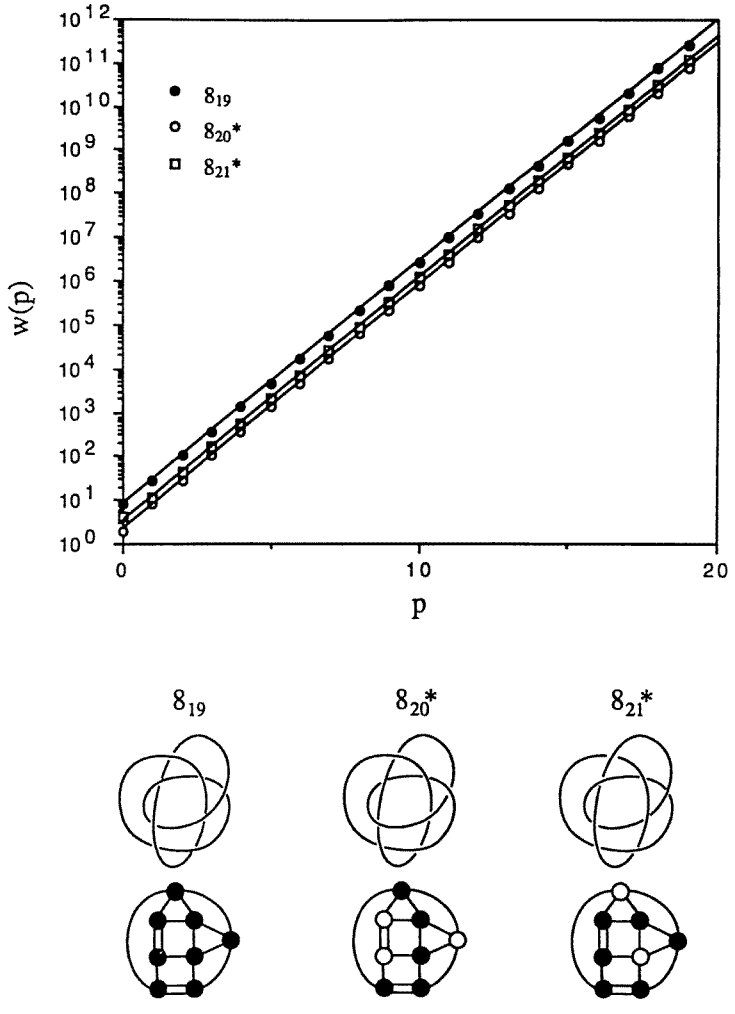

Fig. 11. Linear plot of eq. (6) ($s = 0$) for the illustrated set of similar knot diagrams and their vertex-bicolored graphs. Provenance of diagrams and parameters of plots are listed in table 16.

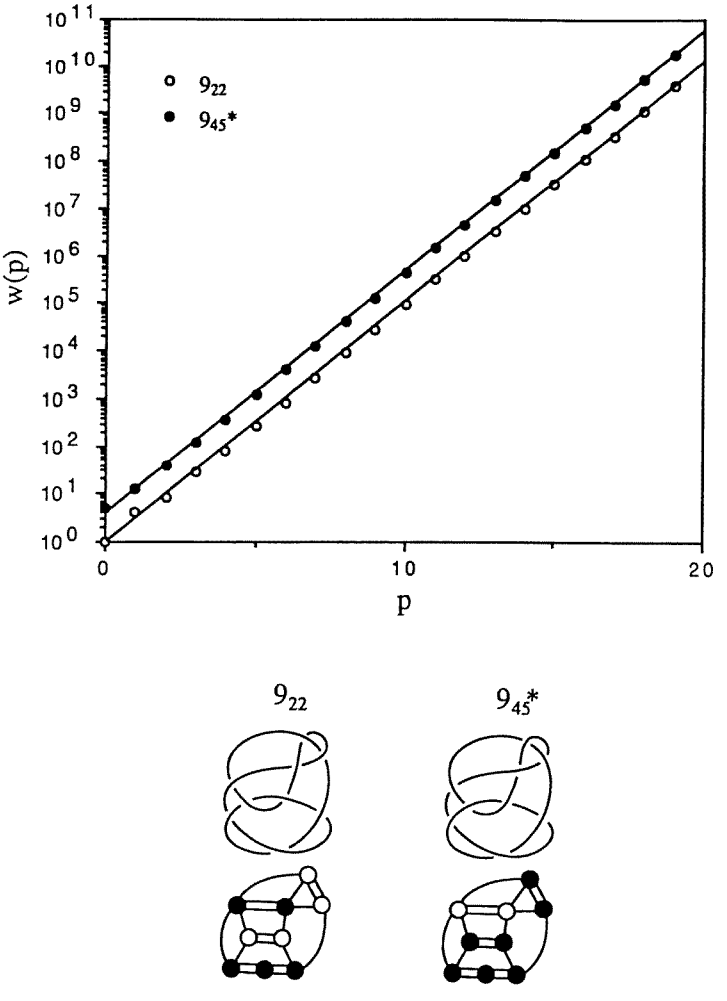

Fig. 12. Linear plot of eq. (6) ($s = 0$) for the illustrated set of similar knot diagrams and their vertex-bicolored graphs. Provenance of diagrams and parameters of plots are listed in table 16.

diagram polymorphism. Thus, two different (though isotopic) diagrams of the same knot, for example 8_{19}, belong to two different sets of similar (in the sense defined above) diagrams (figs. 10 and 11). The same is true of 8_{20} (figs. 10 and 11), 9_{45} (figs. 12 and 13), and 9_{44} (figs. 13 and 14). A given knot may therefore give rise to two or more linear plots with very different slopes, depending on which diagram is chosen. An extreme example is 8_{20}, for which Tait has shown 5 different diagrams [17], including the two in figs. 10 and 11 and the "bowline knot" in fig. 5.

While different diagrams with a common knot graph yield linear plots with

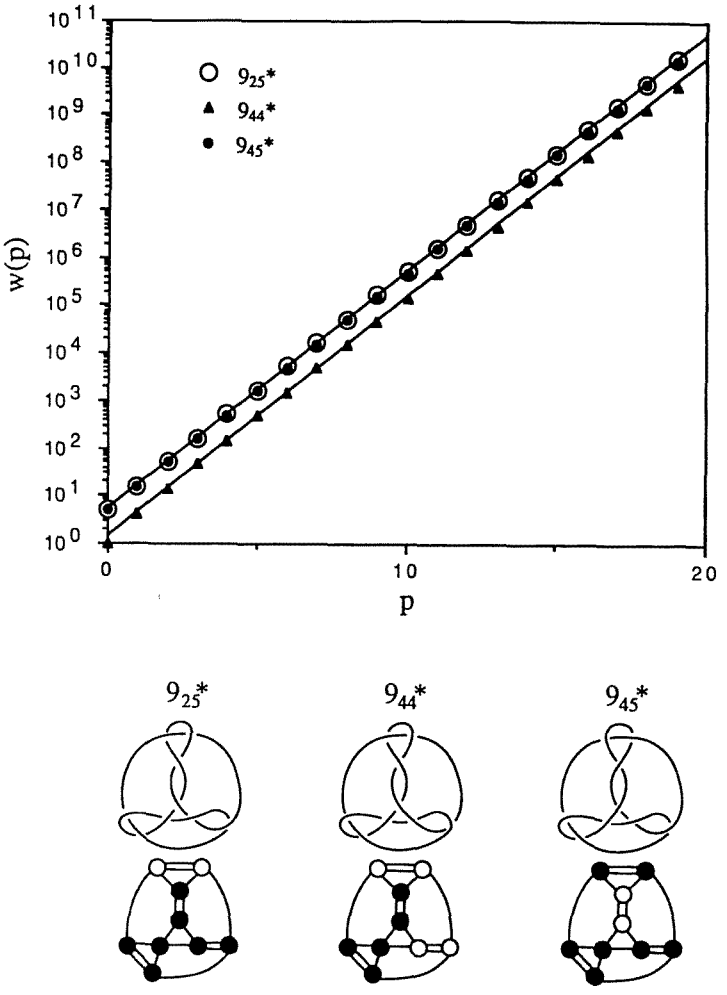

Fig. 13. Linear plot of eq. (6) ($s = 0$) for the illustrated set of similar knot diagrams and their vertex-bicolored graphs. Provenance of diagrams and parameters of plots are listed in table 16.

(nearly) the same slope, the converse is decidedly not the case: parallel lines do not necessarily imply a common knot graph. Consider, for example, the remarkable sameness in the *absolute* values of the writhe profiles (up to w_5) for 12_{1199} and 12_{1231} (table 15). Despite the fact that the two knots (fig. 9) do not share the same knot graph, linear plots of $\log w_p$, vs. $(p-2)$ ($R^2 = 1.000$ for both) have closely similar parameters: $\{\kappa, w'_s\} = \{0.546, 2.88\}$ for 12^*_{1199} and $\{0.549, 2.80\}$ for 12_{1231}. Interestingly, the two knots share the same black and white subgraphs (fig. 16). However, this is not a necessary condition for parallel plots. For example, the parameters $\{\kappa, w'_s\} = \{0.447, 3.44\}$ of the linear ($R^2 = 1.000$) plot for 8^*_6 make it a candidate for placement with the set in fig. 10, yet neither the knot graph nor its subgraphs (fig.

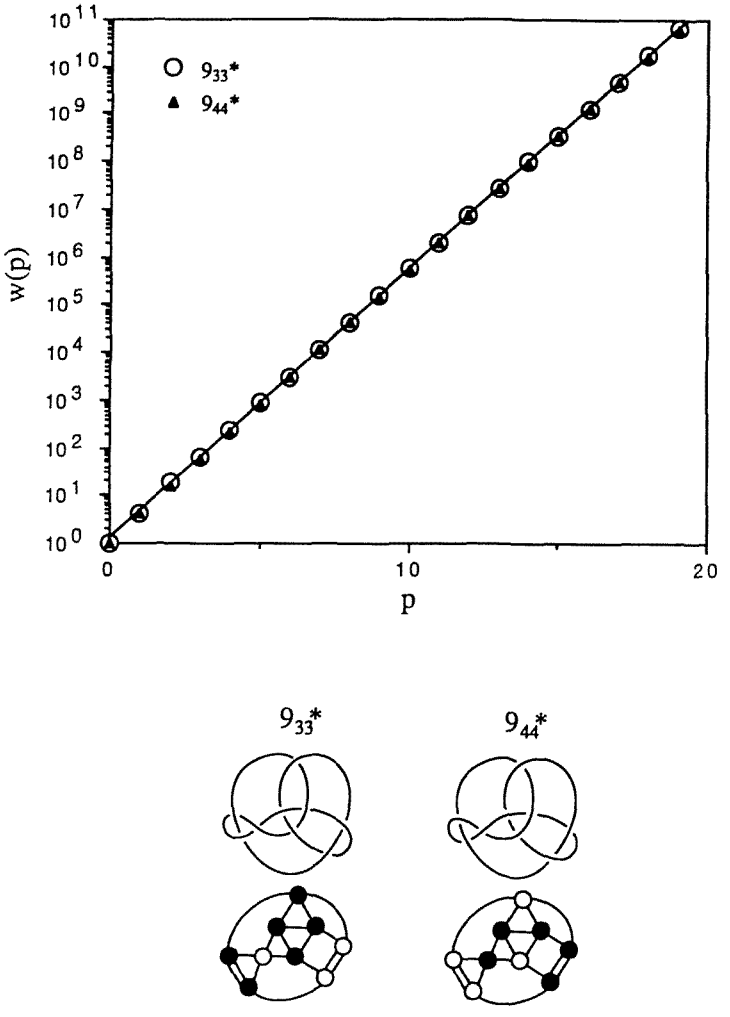

Fig. 14. Linear plot of eq. (6) ($s = 0$) for the illustrated set of similar knot diagrams and their vertex-bicolored graphs. Provenance of diagrams and parameters of plots are listed in table 16.

16) bear any reasonable relationship to the others in the set.

The magnitude of κ depends to a significant extent on f, the average of the vertex coordination numbers in the knot graph:

$$f = \frac{1}{N}\sum_{i=1}^{N} \delta_i \tag{7}$$

Fig. 17 shows that κ increases roughly as a function of $\log f$, but other factors

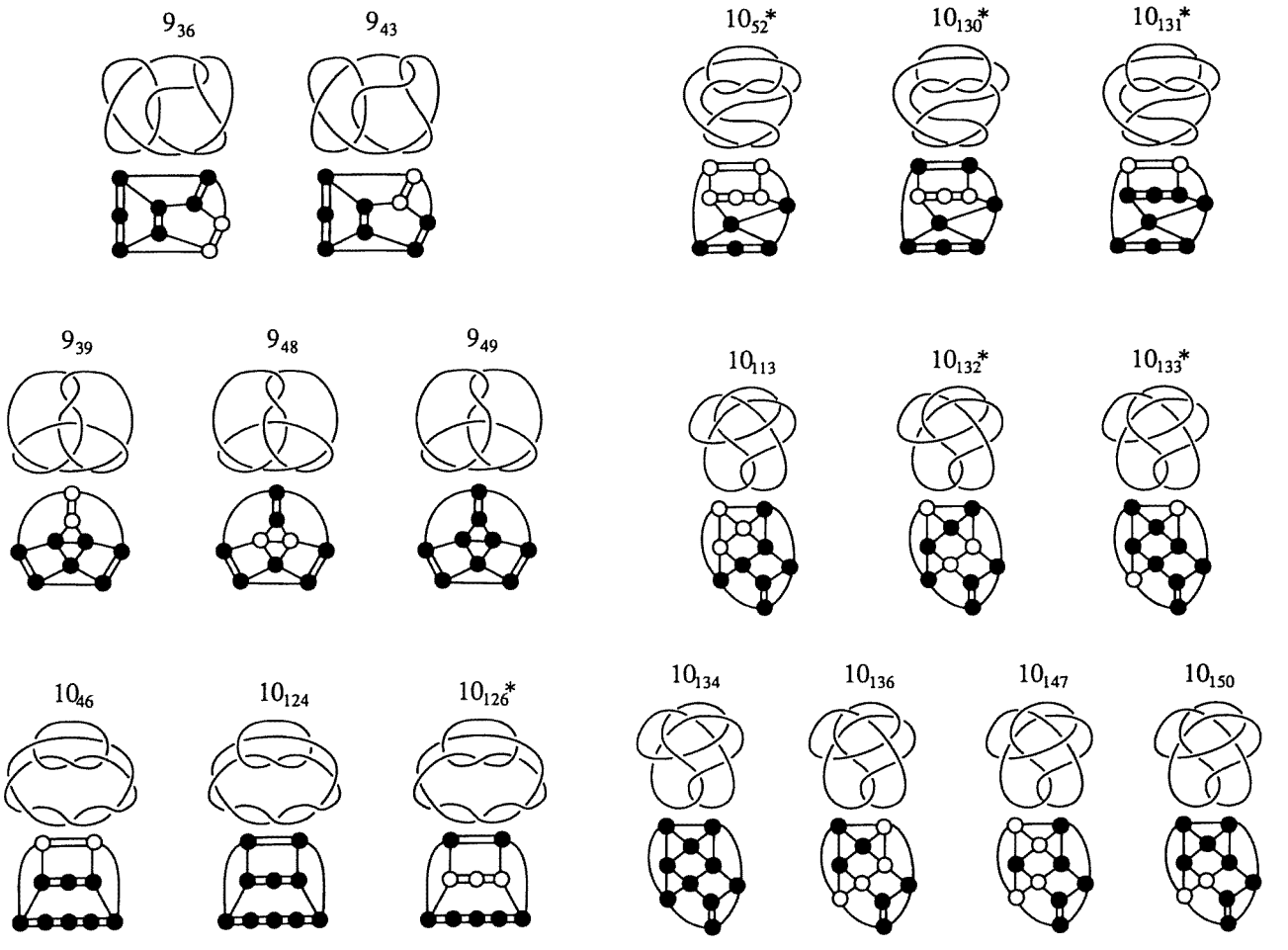

Fig. 15. Additional sets of similar knot diagrams and their vertex-bicolored graphs. Provenance of diagrams and parameters of linear plots are listed in table 16. *Fig. 15 continues on next page.*

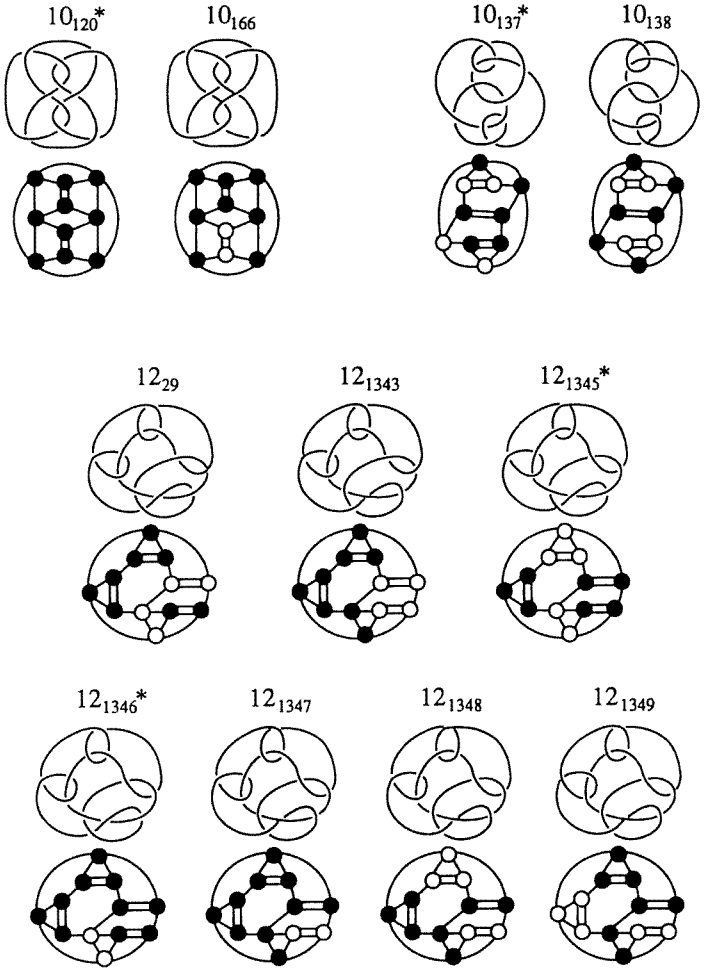

Fig. 15 (continued from previous page).

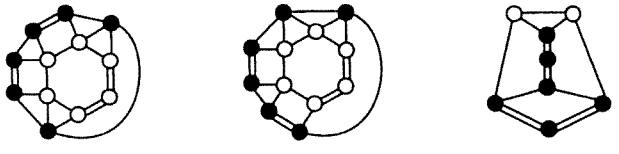

Fig. 16. Vertex-bicolored knot graphs of 12^*_{1199} (left), 12_{1231} (center), and 8^*_6 (right). Asterisks denote enantiomorphs of the knots in [9,10].

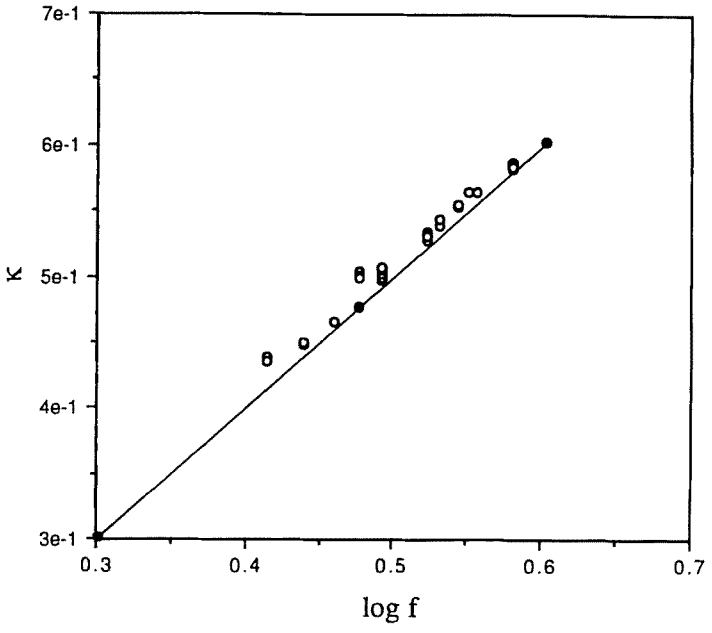

Fig. 17. Plot of $\log f$ vs. κ. The three filled circles represent regular knot graphs ($\kappa = \log f$, straight line segment) and the open circles represent graphs of the knots in table 16. Individual values of κ and $\log f$ are given in table 16.

obviously also play a role. Notably, $\kappa = \log f$ only for regular graphs; for all others; $\kappa > \log f$.

Acknowledgements

Support of this project by the National Science Foundation is gratefully acknowledged. We are much obliged to Morwen Thistlethwaite for his kindness in providing us with unpublished listings of knots and their polynomials, and for permission to cite this work.

References

[1] W.T. Kelvin, *Baltimore Lectures on Molecular Dynamics and the Wave Theory of Light* (C.J. Clay, London, 1904) p. 619.
[2] E. Ruch, Theor. Chim. Acta (Berl.) 11 (1968) 183;
E. Ruch, Acc. Chem. Res. 5 (1972) 49.
[3] S.J. Tauber, J. Res. Nat. Bur. Stand. 67A (1963) 591.
[4] K. Murasugi, Topology 26 (1987) 187;
M.B. Thistlethwaite, Topology 27 (1988) 311.

[5] E. Flapan, Topological techniques to detect chirality, in: *New Developments in Molecular Chirality*, ed. P.G. Mezey (Kluwer Acad. Publ., Dordrecht, 1991) pp. 209–239.
[6] V. Prelog and G. Helmchen, Angew. Chem. Int. Ed. Engl. 21 (1982) 567, and references therein.
[7] G. Schill, *Catenanes, Rotaxanes, and Knots* (Academic Press, New York, 1971) p. 18.
[8] D.M. Walba, Tetrahedron 41 (1985) 3161.
[9] D. Rolfsen, *Knots and Links* (Publish or Perish, Berkeley, 1976; second printing with corrections: Publish or Perish, Houston, 1990), Appendix C: Table of knots and links, pp. 388–429.
[10] M.B. Thistlethwaite, unpublished results.
[11] C. Liang and Y. Jiang, J. Theor. Biol. 158 (1992) 231.
[12] C. Liang and K. Mislow, J. Math. Chem. 15 (1994) 1.
[13] K. Mislow and M. Raban, Stereoisomeric relationships of groups in molecules, in: *Topics in Stereochemistry*, Vol. 1, eds. N.L. Allinger and E.L. Eliel (Wiley, New York, 1967) pp. 1–38;
K. Mislow and J. Siegel, J. Amer. Chem. Soc. 106 (1984) 3319.
[14] O. Frank, *Statistical Inference in Graphs* (Foa Repro, Stockholm, 1971) pp. 26–30.
[15] T.A. Brown, J. Combin. Theory 1 (1966) 498;
F. Harary and E.M. Palmer, *Graphical Enumeration* (Academic Press, New York, 1973) pp. 231–233.
[16] G. Burde and H. Zieschang, *Knots* (Walter de Gruyter, Berlin, 1985), fig. 14.12, p. 265.
[17] P.G. Tait, On knots I, II, III, *Scientific Papers Vol. I* (Cambridge University Press, London, 1898) pp. 273–347. Plates V and VII.
[18] R.H. Crowell and R.H. Fox, *Introduction to Knot Theory* (Blaisdell, New York, 1963) p. 132.
[19] J.H. Conway, An enumeration of knots and links, and some of their algebraic properties, in: *Computational Problems in Abstract Algebra*, ed. J. Leech (Pergamon Press, New York, 1970) pp. 329–358; fig. 8, p. 335.
[20] For an overview, see: K.C. Millett, Algebraic topological indices of molecular chirality, in: *New Developments in Molecular Chirality*, ed. P.G. Mezey (Kluwer Acad. Publ., Dordrecht, 1991) pp. 165–207.
[21] M.B. Thistlethwaite, Knot tabulations and related topics, in: *Aspects of Topology*, London Math. Soc. Lecture Note Series no. 93, eds. I.M. James and E.H. Kronheimer (Cambridge University Press, Cambridge, 1985) pp. 1–76.